Int J Adv Manuf Technol (2016) 87:2673–2682
DOI 10.1007/s00170-016-8600-x

ORIGINAL ARTICLE

Prediction model of depth of penetration for alumina ceramics turned by abrasive waterjet—finite element method and experimental study

Dun Liu[1] · **Hongtao Zhu**[1] · **Chuanzhen Huang**[1] · **Jun Wang**[1] · **Peng Yao**[1]

Received: 17 September 2015 / Accepted: 2 March 2016 / Published online: 1 April 2016

Abstract Many finite element (FE) models for the impacts of ultrahigh-velocity micro-particles on ductile materials have been developed in the recent years. However, few FE models on brittle materials were found from the literatures. This paper presented an attempt to model the ultrahigh-velocity (417–528 m/s) impact process for alumina ceramics. The methodology involved the FE method analysis to estimate the volume of material removal based on the Johnson–Holmquist ceramic material (JH-2) model. Subsequently, the depth of penetration (DOP) on various abrasive waterjet (AWJ) turning parameters was predicted by the FE models and derived mathematical equations. The final depths of penetration predicted by the FE models were found to be in good agreement with the experimental results. The average relative error between the predicted and experimental results was lower than 15 %. Furthermore, the preliminary mechanism of ceramic material removal was analyzed from the FE models. Under ultrahigh-velocity impact, the ceramic material removal stemmed from the initiation and propagation of the cracks. The large-scale ceramic material removal was caused by the crack coalescence. Thus, the DOP on AWJ turning process can be effectively predicted by the FE models. Expectantly, this paper will supply a guidance to select a proper method for predicting the AWJ turning process.

Chuanzhen Huang is a visiting Professor at The University of New South Wales, UNSW, Australia

✉ Chuanzhen Huang
chuanzhenh@sdu.edu.cn

[1] Center for Advanced Jet Engineering Technologies (CaJET), Key Laboratory of High-efficiency and Clean Mechanical Manufacture (Ministry of Education), School of Mechanical Engineering, Shandong University, Jinan 250061, China

Keywords Abrasive waterjet turning · Depth of penetration · Finite element method · Prediction model

1 Introduction

As presented by Wang [1] and Axinte et al. [2], abrasive waterjet (AWJ) machining technology has been found to be one of the most advanced nontraditional machining methods used in the industry for parting cuts on brittle materials like ceramics with the distinct advantages of negligible thermal effects and extremely low cutting force. As discussed by Ali [3] and Wang [4], the advantages of AWJ over other machining processes are particularly beneficial to turning. Compared with conventional turning lathe, the numerous axi-symmetric shapes might be achieved by only a universal tool (the abrasive jet).

As shown by Çaydaş and Hasçalık [5], the AWJ machining process is a complicated nonlinear process. The experimental methods generally require a large number of trials due to more considered machining parameters. However, a great deal of experimental data is necessary for obtaining the suitable analytical model.

Compared to both experimental method and analytical method, finite element (FE) method is a typically numerical technique to find the approximate solution to the very complicated problem.

Various FE modeling erosion models of single-particle-target impact have been presented.

Eltobgy et al. [6] presented an elasto-plastic finite element model to simulate the erosion process in 3D configuration. This model offered the opportunity to study the effects of the particle size, velocity, and impact angle on contact time. Junkar et al. [7] used the ANSYS/LS-DYNA FE software to investigate the effect of single-particle impact on the crater

roundness at the surface of AISI 304 in abrasive water jet machining. The velocities (180–220 m/s) of the impacting particles used in the FE model were not within the experimental range (350–550 m/s) expected to occur in real AWJ processes investigated by Balz and Heiniger [8], and this can lead to inaccuracies when calculating the momentum of the impacting particles. Compared with the Zeng and Kim's model [9], Gudimetla and Yarlagadda [10] developed a more accurate model using FE analysis to predict the erosion rates due to selecting an appropriate coefficient of restitution. However, not considering the actual particle size, whether the FE model can be scaled down or not is puzzled. Wang and Yang [11] developed FE erosion models for both ductile and brittle materials. The model is available to calculate the 3D computational model and the cases with different particle diameters. One of the considerable superiorities of this FE model was convenient to measure the residual stress which was difficult to be acquired by experimental method. Takaffoli and Papini [12] presented a 2D FE model of impact process on a copper target with rigid rhomboid particles. It was finally found that the deleted element approach gave the best accordance with experimental results. Answar et al. [13] presented a FE model of a single-particle impact during AWJ milling. The FE model was carefully developed by experimental procedure that provided data on single-particle impact on the target workpiece. It enabled the validation of the proposed model. Li et al. [14] focused on studying the material (AISI 4340 steel) response to the ultrahigh-velocity (350–700 m/s) impact by the single micro-particle using the FE method based on a modified Johnson–Cook constitutive model. Compared with the experimental results, it was found that the FE model can predict the AWJ process believably. Lv et al. [15] investigated the erosion process of AlN ceramics in ultrasonic-assisted AWJ machining using an explicit dynamic FEM. The results showed that the maximum erosion rate of blunt and sharp impact particles can be acquired with the impact angle of 90° and 30°, respectively.

Although many attempts have been conducted to model the impact process of single-particle target, there were several limitations in previous studies. Many FE models (e.g., found in [6, 7, 11, 12, 15]) focused on simulation of low-velocity impact process. Few FE models (e.g., found in [13, 14]) were put forward and validated by ultrahigh-velocity impact experiments simultaneously. Much work (e.g., found in [6, 7, 12–14]) only considered the modeling of solid particle erosion in ductile materials using various FE methods and did not consider brittle materials. Most of all, it is not found that predicting the AWJ turning process using the FE method in previous studies.

Aiming at the above mentioned limitations on AWJ machining, this paper attempted to study the predicted model of AWJ turning alumina ceramics based on the FE method. The methodology involved the FE method analysis to estimate the volume of material removal by ultrahigh-velocity (417–528 m/s) impact based on the Johnson–Holmquist ceramic material (JH-2) material model. Subsequently, the depth of penetration (DOP) on various AWJ turning parameters was predicted by the FE models in combination with derived mathematical equations. The results of the FE models were compared and validated with our own AWJ turning experiments. It will supply a guidance to select a proper method for predicting the AWJ turning process.

2 Theoretical basis

2.1 Estimation of velocity of abrasive particle

As introduced by Ali [3] and Fox et al. [16], for an ideal potential fluid, under one-dimensional steady state flow conditions, the energy is conserved. According to Bernoulli's equation,

$$\frac{P_i}{\rho_i}+\frac{v_i^2}{2}=\frac{P_o}{\rho_o}+\frac{v_o^2}{2} \tag{1}$$

where P is the hydrostatic pressure, v is the average velocity of the stream, and ρ is the fluid density. The subscripts i and o refer to the inlet and outlet of the flow, respectively. Thus, the v_o can be solved as illustrated in Eq. (2):

$$v_o \approx \sqrt{\frac{2P_i}{\rho}} \tag{2}$$

Considering the loss of momentum produced by friction, the velocity of waterjet v_w can be defined by Eq. (3):

$$v_w=\kappa\sqrt{\frac{2P_i}{\rho}}=1.2445\sqrt{1000p_i}=39.355\sqrt{p_i} \tag{3}$$

As shown by Momber and Kovacevic [17] and Hashish [18], typical values for κ based on jet force measurements are ranged from 0.83 to 0.93. Because the pressure ranges from 200 to 320 MPa, the 0.88 is selected as the κ value.

Under the law of momentum conservation, the equation is described as follows:

$$\dot{m}_w.v_w=\left(\dot{m}_a+\dot{m}_w\right).v_p \tag{4}$$

where $\dot{m}_a$ is the abrasive mass flow rate and $\dot{m}_w$ is the water mass flow rate.

Therefore, the particle velocity v_p can be written as shown in Eq. (5):

$$v_p=\frac{v_w}{1+\dot{m}_a/\dot{m}_w} \tag{5}$$

The efficiency of the abrasive-particle acceleration is between 0.65 and 0.85. Thus, the middle value 0.75 is selected as the efficiency of momentum transfer χ value. The real particle velocity v_{pr} can be expressed as in Eq. (6):

$$v_{pr} = \frac{\chi v_w}{1 + \dot{m}_a/\dot{m}_w} \tag{6}$$

Since a very small number of particles have been used in each test, the mass ratio term (m_a/m_w) in Eq. (6) is neglected. The final real velocity of particle can be illustrated as in Eq. (7):

$$v_{pr} = \frac{\chi v_w}{1 + \dot{m}_a/\dot{m}_w} \approx 0.75 v_w = 29.52\sqrt{P_i} \tag{7}$$

According to Eq. (7), Fig. 1 shows the relationship of the real particle velocities versus the waterjet pressure (ranging from 200 to 320 MPa).

2.2 Derivation of the final depth of penetration

As defined by Manu and Babu [19], the volume of material removal during each turning revolution can be evaluated from the rectangular block like the developed FE model. The length is equal to the circle circumference of the workpiece, the width is equal to the jet diameter D_j, and the height is equal to the radial DOP during that particular revolution.

Thus, the radial DOP of jet for the ith revolution is given by Eq. (8):

$$dr_i = \frac{V_i}{\pi \times D_i \times D_j} \tag{8}$$

where V_i is the volume of material removal during the ith revolution and D_i is the initial workpiece diameter of the ith revolution.

The workpiece rotated at a rotational speed N revolutions per minute and the jet traversed along the workpiece axis with the speed v_t (mm/s) simultaneously. Thus, the number of revolutions n_p is represented by Eq. (9):

$$n_p = N \times D_j / v_t \tag{9}$$

As illustrated by Finnie [20], the coefficient c (equating to 0.5) was introduced to consider the effect of the multiple-impact in AWJ machining.

It was assumed that the volumes of removed materials by multiple impacts were considered as the accumulated volume by single impact (V_s). In our study, the V_s can be acquired by the developed FE model results. Thus, the V_i will be described as in Eq. (10):

$$V_i = c \times \dot{m}_a \times V_s \times 60/N \tag{10}$$

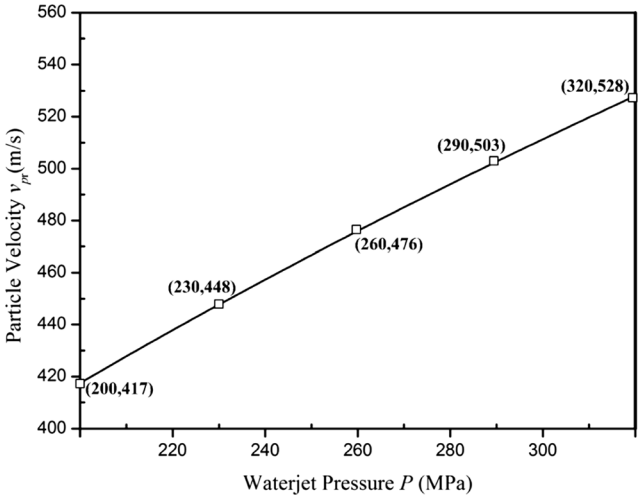

Fig. 1 Real particle velocities versus waterjet pressure

Then, the workpiece diameter at the $(i+1)$th revolution can be expressed as Eq. (11):

$$D_{(i+1)} = D_i - 2 \times dr_i \tag{11}$$

The Eq. (10) was substituted in Eq. (8) and (11).

Finally, after the n_p revolutions, the DOP can be illustrated by Eq. (12):

$$DOP = \left(D_{initial} - D_{final}\right)/2 \tag{12}$$

where the $D_{initial}$ and D_{final} are the initial diameter and final diameter of workpiece (after the n_p revolutions), respectively.

2.3 Alumina ceramic materials model

The JH-2 constitutive model was proposed to describe the response of ceramic materials to large strain rate. The JH-2 constitutive model requires several material constants to completely describe the response of a particular ceramic material. A detailed description can be found in the literatures by Johnson and Holmquist [21], Cronin et al. [22], and Hallquist [23].

The equivalent stress for a ceramic material is given in terms of the damage parameter D by Eq. (13):

$$\sigma^* = \sigma_i^* - D\left(\sigma_i^* - \sigma_f^*\right) \tag{13}$$

The intact material strength is defined as in Eq. (14):

$$\sigma_i^* = A\left(P^* + T^*\right)^N \left(1 + C\ln\dot{\varepsilon}^*\right) \tag{14}$$

where the superscript "*" indicates a normalized quantity. Thus, the $\dot{\varepsilon}^*$ is the normalized plastic strain rate, T* is the normalized maximum tensile strength, P* is the normalized pressure, A is the intact normalized strength parameter, C is

Table 1 JH-2 model material constants for alumina materials 99.5 % from Krashanitsa [24]

Materials properties	Symbol	Alumina
Density	ρ (kg/m^3)	3850
Shear modulus	G (GPa)	123
JH-2 normalized intact strength coefficient	A	0.949
JH-2 normalized fractured strength coefficient	B	0.1
JH-2 strain rate constant	C	0.007
JH-2 fractured strength exponent	M	0.2
JH-2 intact strength exponent	N	0.2
Tensile strength	T*(GPa)	0.262
Normalized fracture strength	SFmax	1e20
Hugoniot elastic limit (HEL)	HEL (GPa)	8
HEL pressure	pHEL (GPa)	1.46
HEL strength	THEL (GPa)	2.0
JH-2 damage constant	D1	0.001
JH-2 damage constant	D2	1.0
Bulking factor	β	1.0
JH-2 pressure constant	K1 (GPa)	186.8
JH-2 pressure constant	K2 (GPa)	0
JH-2 pressure constant	K3 (GPa)	0

the strength parameter for strain rate dependence, and N is the material constant.

The fractured material strength is described as in Eq. (15):

$$\sigma_f^* = B\left(P^*\right)^M\left(1 + C\ln\dot{\varepsilon}\right) \tag{15}$$

where B is the normalized fractured material strength and M is the material constant.

The μ and the pressure P can be calculated as in Eq. (16) and (17), respectively:

$$\mu = \frac{\rho}{\rho_0} - 1 \tag{16}$$

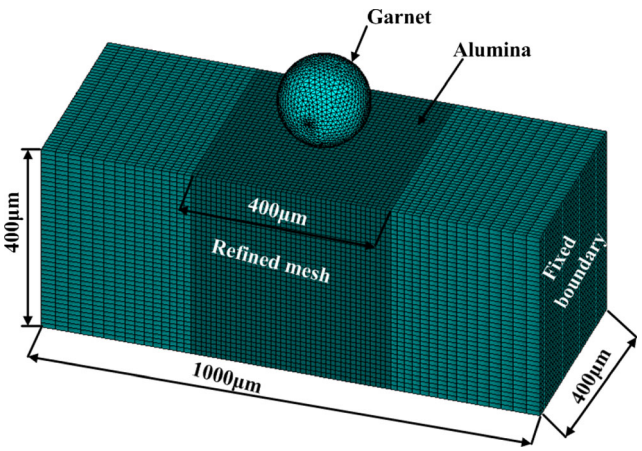

Fig. 2 Model geometry, mesh type, and boundary condition

Table 2 Material constants for garnet from Anwar et al. [25]

Density	4120 kg/m^3
Young's modulus	248 GPa
Poisson's ratio	0.3
Tensile failure stress	150 MPa

where ρ is the current density and ρ_0 is the initial density

$$P = K_1\mu + K_2\mu^2 + K_3\mu^3 \tag{17}$$

In Eq. (17), K_1, K_2, and K_3 are constants (K_1 is the bulk modulus).

The JH-2 constitutive model has been implemented in LS-DYNA as material 110 (*MAT_JOHNSON_HOLMQUIST_CERAMICS). The simulated results can be viewed using the LS-PrePost software.

Alumina material model constants of 99.5 % have been characterized, as shown in Table 1. Since many constants cannot be acquired directly, the actual constitutive constants for a particular material are usually inferred from the manufacturer or published literatures.

3 FE modeling

The geometry of the target was modeled as a rectangular block shown in Fig. 2. The dimensions of the target were $1000 \times 400 \times 400$ μm^3. The boundary conditions for the target were defined as follows: Nodes impacted by a particle on the top face of the target were set free, while nodes on all the other five exterior faces of the target were fixed. A more refined mesh was used in the vicinity of the impact on the target, while a relatively coarse mesh was applied away from the impact area.

The abrasive particle was modeled as a sphere using rigid 3D solid (tetrahedral) elements, with properties shown in Table 2.

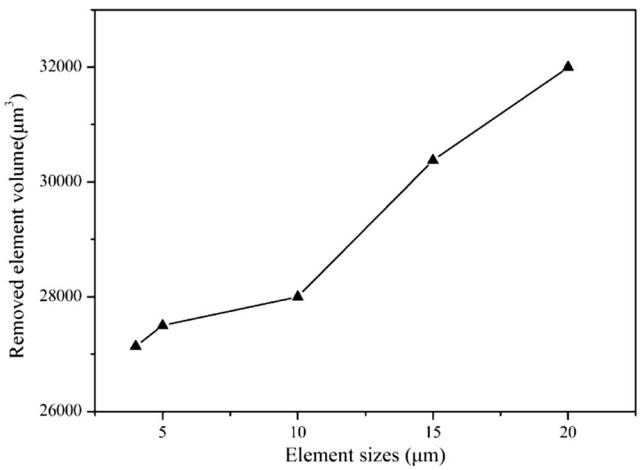

Fig. 3 Removed element volume versus element sizes (at 90° impact angle and 550 m/s impact speed)

Table 3 Process parameters setup in FE simulations

Parameter	Value
V_{pr}, particle velocity at the impact (m/s)	417, 448, 476, 503, 528
α, impact angle (degree)	30, 45, 60, 75, 90

Considering the computation time and accuracy, an appropriate element size for the model needs to be determined. Figure 3 shows the removed element volume results of the mesh sensitivity analysis for different element sizes (5, 10, 15, and 20 μm). Considering the computational accuracy and removed volume errors due to element size, a 4-μm-length element was added to analyze the mesh sensitivity. As shown in Fig. 3, compared with element sizes from 4, 5, and 10 μm, a 5-μm mesh size is finally chosen for its moderate computation time and relatively high accuracy.

The critical time interval that played an important role in FE simulation is used by ANSYS/LS-DYNA to verify if a contact was established between the abrasive particle and the workpiece. From the study of Eltobgy et al. [6], the explicit procedure requires a time interval less than the critical time interval $\triangle t_{cr}$. $\triangle t_{cr}$ can be computed as in Eq. (18):

$$\Delta t_{cr} = \frac{L_e}{\sqrt{\frac{E}{\rho(1+\nu)}}} \tag{18}$$

where L_e is the length of the element, E is the elastic modulus, ρ is the material density, and ν is the Poisson's ratio.

After every time interval is verified, the contact between the abrasive particle and the target surface takes place. The "surface to surface" was chosen as the type of contact in this study. The coefficient of friction is assumed to be 0.1 between the particles and the target surface based on the work of Meo et al. [26] and Meguid et al. [27].

Table 3 gives the summary of process parameters setup in FE simulations.

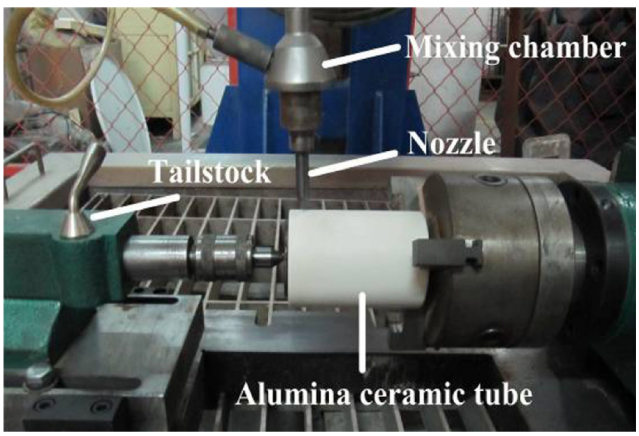

Fig. 4 Experimental setup of the AWJ turning process

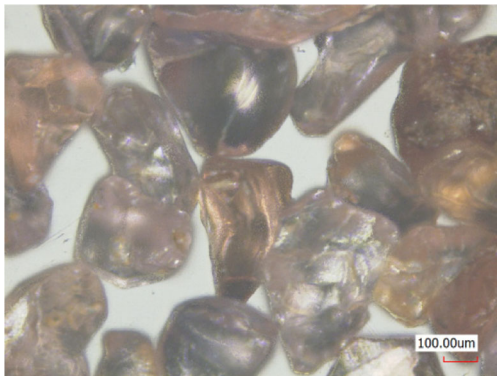

Fig. 5 Sample of garnet particles

In the FE model, the removed volume of workpiece was calculated by multiplying the number of removed elements with the volume of each element.

4 Experimental setup

In the experiments, the workpiece material is a kind of alumina ceramic round tube grounded by diamond grinding wheels before the AWJ turning. The arrangement of the setup on the machine for conducting the turning experiments with AWJ is shown in Fig. 4. A Flow International waterjet cutting system is used, which is equipped with a single intensifier pump that can deliver a waterjet pressure of up to 413 MPa, using an orifice of 0.25 mm in diameter. The nozzle used is 0.76 mm in diameter and 76.2 mm in length, and its motion is controlled by an ABB six-axis robotic arm. As shown in Fig. 5, mesh size #80 garnet abrasives were used for all the turning tests. The average particle diameter is equal to 0.18 mm and the average particle mass is equal to 1.22145×10^{-5} g.

According to the manufacturer's declaration, the mechanical properties of the investigated alumina ceramics are given in Table 4.

As shown in Table 5, six main process parameters considered in this study included traverse speed (v_t), waterjet pressure (p), standoff distance (h), impact angle (θ), surface speed (v_s), and abrasive flow rate ($\dot{m}_a$).

Keyence VK-X200 was used for measuring the DOP, which was measured at four positions on each surface at the

Table 4 Mechanical properties of alumina ceramics tube

Shape: round tube	Density: 3.85 g/cm^3	Vickers hardness: 12 GPa
Diameter: 68 mm	Poisson's ratio: 0.22	Bending strength: 400 MPa
Elastic modulus:350 GPa	Compressive strength: 2500 MPa	Fracture toughness: 4.1 MPa.m$^{1/2}$

Table 5 Parameter design

Symbol	Process parameters	Level 1	Level 2	Level 3	Level 4	Level 5
v_t	Traverse speed (mm/s)	0.1	0.2	0.3	0.4	0.5
p	Waterjet pressure (MPa)	200	230	260	290	320
h	Standoff distance (mm)	2	2	2	2	2
θ	Impact angle (degree)	30	45	60	75	90
v_s	Surface speed (m/s)	2	3.5	5	6.5	8
m_a	Abrasive flow rate (g/s)	5	6.67	8.34	10	11.67

medium area of the cut, and the average was determined. Only single-pass turning was considered.

As shown in Fig. 6, the DOP was characterized by the reduction in the radius of the workpiece.

5 Results and discussions

5.1 Effect of particle speed and impact angle on the removed element volume

As illustrated in Fig. 7, particles impacting on the workpiece at different speeds were simulated using the FE model with an impact angle of 90° for the same workpiece and abrasive material. The removed element volume increase, with an increase in the impact velocity, can be explained by the increase of the kinetic energy of the particle. The higher kinetic energy was acquired at higher impact velocity. As the abrasive impacts the target with higher impact velocity, the abrasive could transfer enough energy to the target. The removed critical energy of materials was achieved. More materials were removed from the target.

Figure 8 shows the relationship between the removed element volume and the impact angle. As the abrasive impacts the target with an inclined angle, the impact velocity can be divided into two components—horizontal component (along the x-direction) and vertical component (along the y-direction). The increasing trend of the removed element volume can be interpreted by the increasing vertical component of the impact velocity. With higher impacting angles, higher vertical component of the impact velocity exists, causing higher material removal. When the inclined angle declines, the vertical component of the impact velocity also decreases. Thus, the abrasive does not have enough kinetic energy to remove the materials. However, as the impact angle increases, the increasing rate in the removed volume declines slowly. It was finally found that the maximum removed volume can be acquired at an angle of 90°.

5.2 Erosion on alumina ceramic materials

Associated with the viewpoints of Zurek and Meyers [28] and Wang and Yang [11], Fig. 9 shows the cross-sectional profile at the impact center of alumina ceramics using the FE method. After particle impacting process, there are many subsurface cracks in the impact center of ceramic materials.

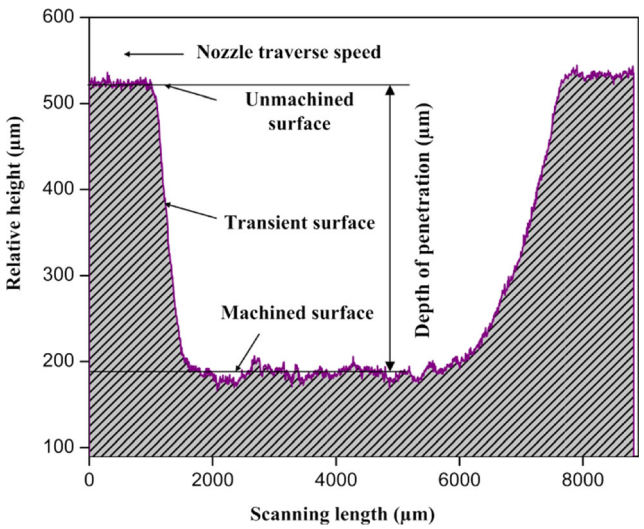

Fig. 6 Sectional view of AWJ turning surface profile

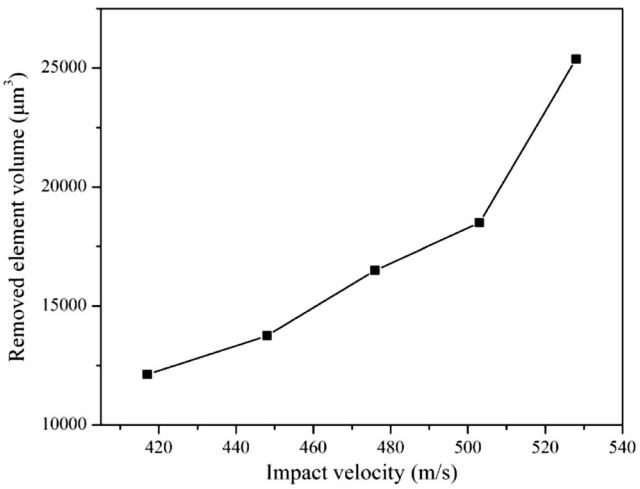

Fig. 7 Removed element volume versus impact velocity when impact angle is equal to 90°

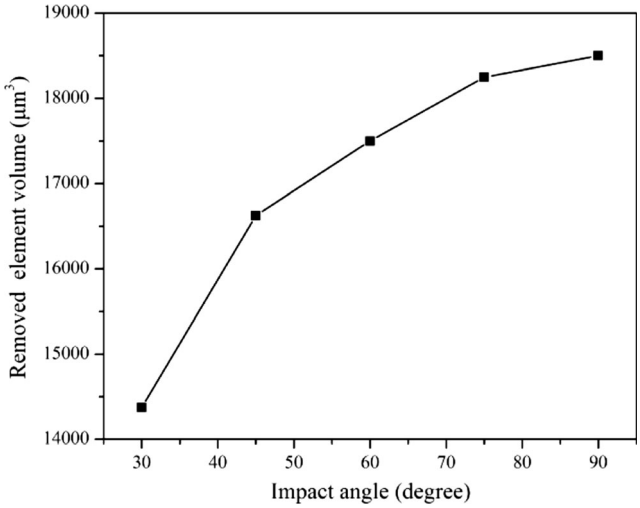

Fig. 8 Removed element volume versus impact angle when impact velocity is equal to 503 m/s

The material removal was related with the normal component of the initial kinetic energy of the particles. As the impact angle increased, the depth of penetration and removed volume of material also obviously increased as shown in Fig. 9a–e. In Fig. 9a, due to the smallest impact angle, the shallowest of depth of penetration is acquired. Therefore, ceramic materials can acquire a maximum removed volume of material at an angle of 90° as shown in Fig. 9e. For ceramic materials, the ceramic material removal stemmed from the initiation and propagation of the cracks and the large-scale ceramic material removal was caused by the crack coalescence. Many small fragments were produced by the dynamic failure. With sufficiently high impact kinetic energy, there was a tendency for cracks to bifurcate, thereby reducing the whole energy of the system. The Wang and Yang's [11] FE results for silicon carbide ceramics gave

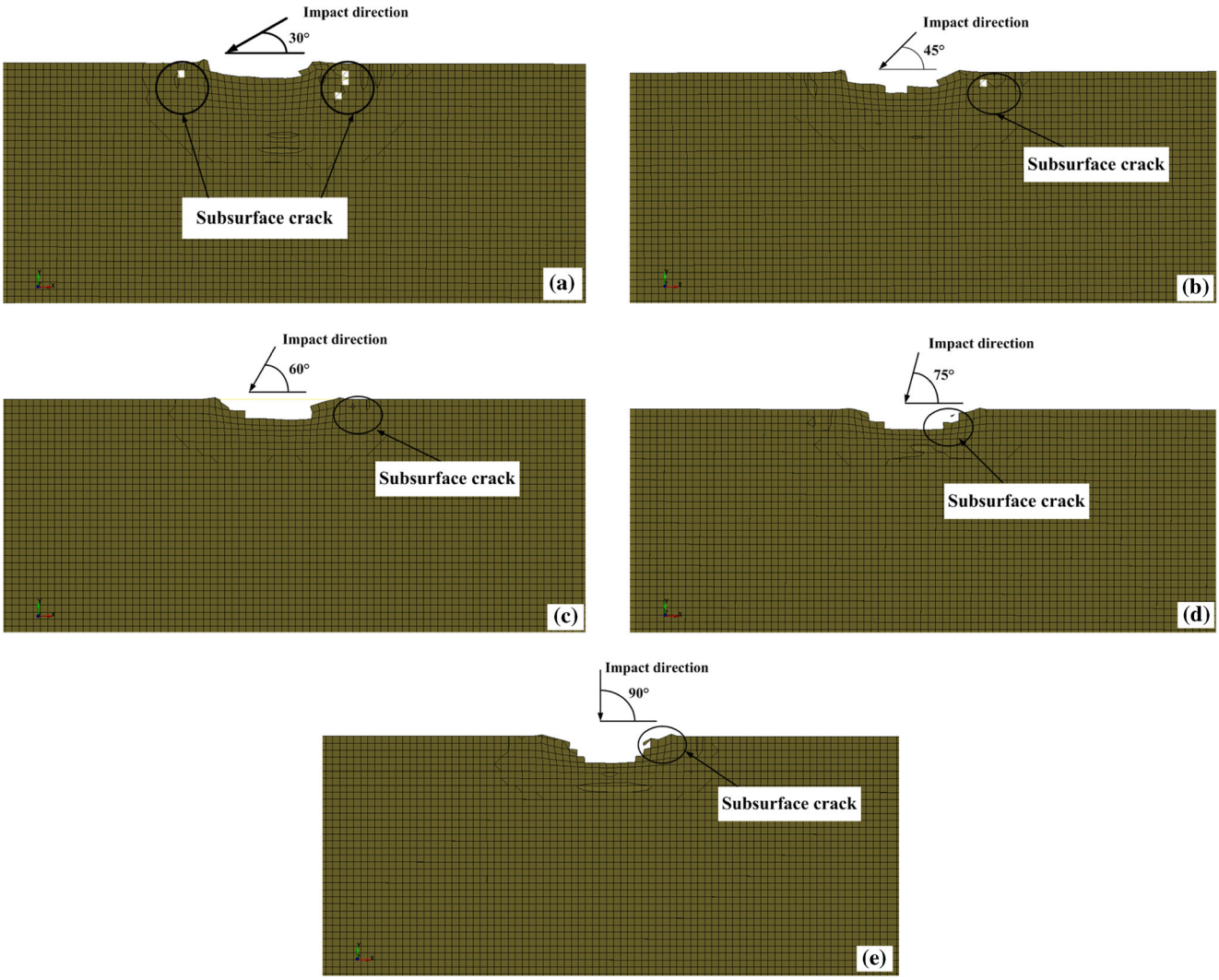

Fig. 9 Cross-sectional profile of alumina ceramics by a single-particle impact at different impacting angles with the same impact velocity (503 m/s). **a** Cross-sectional profile at 30° (smallest impact angle), **b** cross-sectional profile at 45°, **c** cross-sectional profile at 60°, **d** cross-sectional profile at 75°, and **e** cross-sectional profile at 90° (*largest impact angle*)

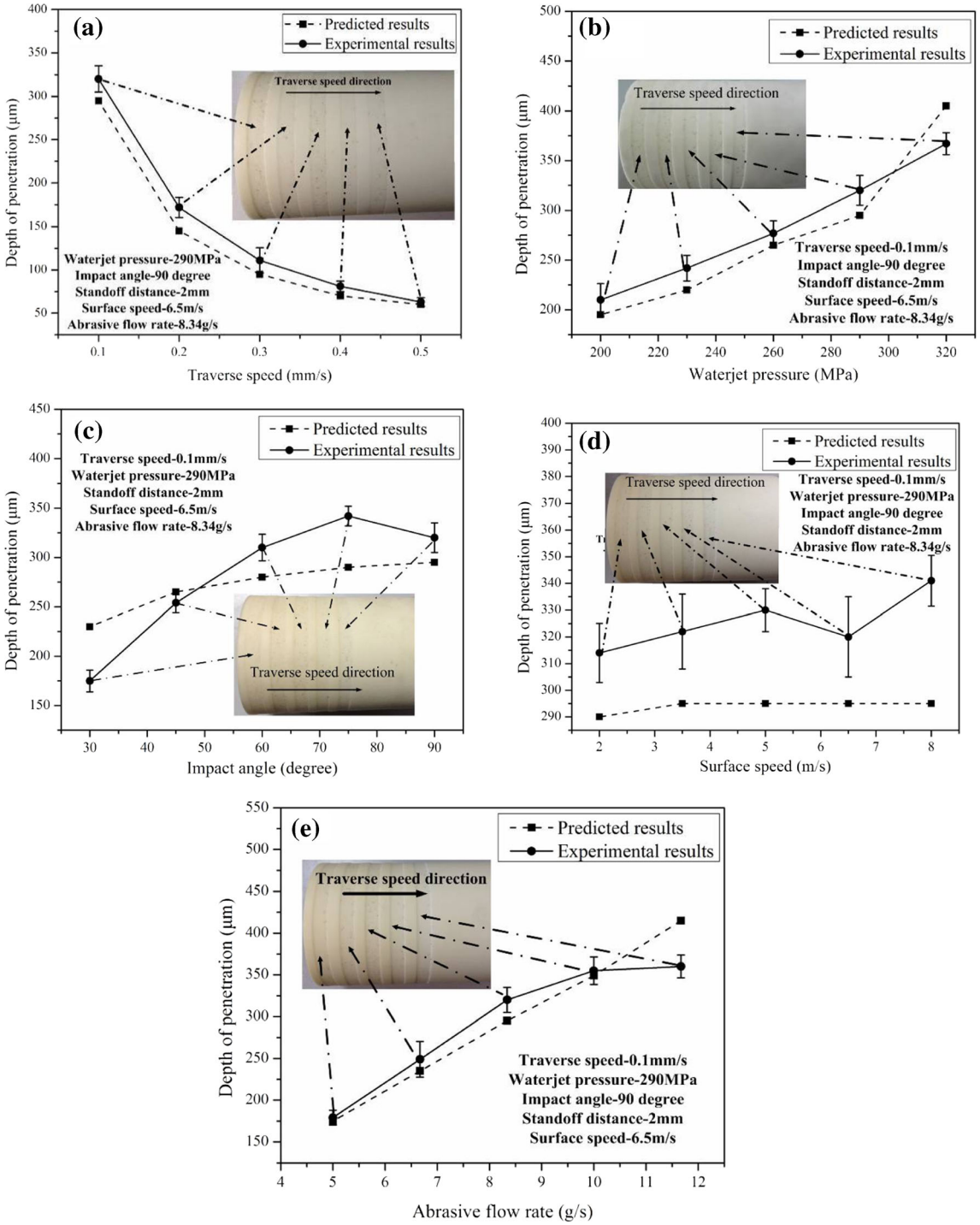

Fig. 10 Depth of penetration versus process parameters. **a** Depth of penetration versus traverse speed, **b** depth of penetration versus water jet pressure, **c** depth of penetration versus impact angle, **d** depth of penetration versus surface speed, and **e** depth of penetration versus abrasive flow rate

the same trend as our presented study. Our presented results were also in agreement with Ćurković et al.'s [29] experimental results. Ćurković et al.'s research results showed that the material removal rate of high-purity alumina ceramics is high at impact angles close to 90°. On account of low fracture toughness, the cracks propagated to form a crack network propagating across the grain boundaries easily.

5.3 Validation of the predicted models by experimental results

In order to check the accuracy of the proposed model, alumina cylindrical tube was considered as desired shape for the workpiece. An assessment of the models has been carried out using the 25 sets of experimental data.

It is shown that the predicted trends from the model for the DOP are in good agreement with the experimental data as shown in Fig. 10. The models present the effects of the DOP versus various process parameters. In Fig. 10a, the predicted tendency and results of the DOP versus traverse speed were highly consisted with the experimental results. The DOP decreases with the increasing of the traverse speed. The changing trend between DOP and waterjet pressure shown in Fig. 10b was in accord with the changing trend between removed element volumes and impact velocity (waterejet pressure) shown in Fig. 7. Meanwhile, the changing trend between DOP and impact angle shown in Fig. 10c was also consistent with the changing trend between removed element volumes and impact angle shown in Fig. 8. In Fig. 10b–e, there were slight fluctuations at some points but predicted tendencies of the DOP versus various process parameters were approximately identical. For instance, in Fig. 10e, the DOP did not increase sharply as the $\dot{m}_a$ increased significantly in practice due to the kinetic energy loss of effective impact particles. There were two main reasons about it: (1) According to the law of conservation of momentum, as the abrasive flow rate increases, the single-particle impact velocity decreases. Simultaneously, compared with abrasive mass, the impact velocity has greater impact on abrasive energy according to the theorem of kinetic energy. (2) Abrasive interference, due to higher abrasive flow rate, leads to the reduction of effective impact particles. Furthermore, the average relative error between the predicted and the corresponding experimental results is lower than 15 %. In summary, it can be stated that the developed FE model can achieve good predictions qualitatively and quantitatively.

6 Conclusions

This paper presents an attempt to model the AWJ turning process considering the DOP for alumina ceramics. The methodology involves finite element method analysis to estimate the DOP. The final DOP, predicted by the FE models, are found to be in good agreement with the experimental results. From the presented work, the following main conclusions can be drawn.

1. The FE model was developed to simulate the single ultrahigh-velocity micro-particle impact process based on JH-2 ceramic model. The removed material volumes versus various impact angles (ranging from 30° to 90°) and impact velocities (ranging from 417 to 528 m/s) were obtained in the FE model. Due to higher normal impact energy, the removed element volumes increase with an increase of the impact velocity and impact angle.
2. Analyzing the cross-sectional profile of alumina ceramics by a single-particle impact at different impact angles from the FE models, the preliminary mechanism of ceramic materials removal was obtained. The ceramic material removal stemmed from the initiation and propagation of the cracks, and the large-scale ceramic material removal was caused by the crack coalescence.
3. The final DOPs predicted by the FE models, in combination with derived equations, are found to be in good agreement with the AWJ turning experimental results. The average relative error between the predicted and the corresponding experimental results was lower than 15 %. Thus, the DOP on AWJ turning process can be effectively predicted by the FE models.
4. Under rather more realistic conditions, various particle shapes (conical, cylindrical particles, etc.), particle size, and multiple-particle impacts should be considered for further research.

Acknowledgments This work is supported by the National Natural Science Foundation of China (51175307, 51375273).

References

1. Wang J (2009) A new model for predicting the depth of cut in abrasive waterjet contouring of alumina ceramics. J Mater Process Technol 209:2314–2320
2. Axinte DA, Karpuschewski B, Kong MC, Beaucamp AT, Anwar S, Miller D, Petzel M (2014) High energy fluid jet machining (HEFJet-Mach): from scientific and technological advances to niche industrial applications. CIRP Ann Manuf Technol 63:751–771
3. Ali YM, Wang J (2011) Impact abrasive machining. In: Jackson MJ, Davim JP (eds) Machining with abrasives. Springer, West Lafayette, pp 385–422
4. Wang J (2003) Abrasive waterjet machining of engineering materials. Trans Tech Publications, Uetikon-Zuerich, Switzerland, p 35
5. Çaydaş U, Hasçalık A (2008) A study on surface roughness in abrasive waterjet machining process using artificial neural networks and regression analysis method. J Mater Process Technol 202:574–582
6. Eltobgy MS, Ng E, Elbestawi MA (2005) Finite element modeling of erosive wear. Int J Mach Tools Manuf 45:1337–1346
7. Junkar M, Jurisevic B, Fajdiga M, Grah M (2006) Finite element analysis of single-particle impact in abrasive water jet machining. Int J Impact Eng 32:1095–1112
8. Balz R, Heiniger KC (2011) Determination of spatial velocity distributions of abrasive particles in abrasive water jets using laser-induced fluorescence under real conditions. In: Proceedings of 16th WJTA-IMCA Conference and Expo, Houston, Texas.
9. Zeng JY, Kim TJ (1996) An erosion model of polycrystalline ceramics in abrasive waterjet cutting. Wear 193:207–217
10. Gudimetla P, Yarlagadda PKDV (2007) Finite element analysis of the interaction between an AWJ particle and a polycrystalline alumina ceramic. J Achiev Mater Manuf Eng 23:7–14
11. Wang Y, Yang Z (2008) Finite element model of erosive wear on ductile and brittle materials. Wear 265:871–878
12. Takaffoli M, Papini M (2009) Finite element analysis of single impacts of angular particles on ductile targets. Wear 267:144–151

13. Anwar S, Axinte DA, Becker AA (2011) Finite element modelling of a single-particle impact during abrasive waterjet milling. Proc Inst Mech Eng J J Eng Tribol 225:821–832
14. Li WY, Wang J, Zhu HT, Li HZ, Huang CZ (2013) On ultrahigh velocity micro-particle impact on steels—a single impact study. Wear 305:216–227
15. Lv Z, Huang CZ, Zhu HT, Wang J, Yao P, Liu ZW (2015) FEM analysis on the abrasive erosion process in ultrasonic-assisted abrasive waterjet machining. Int J Adv Manuf Technol 78:1641–1649
16. Fox RW, McDonald AT, Pritchard PJ (2003) Introduction to fluid mechanics, 6th edn. Wiley, Hoboken, pp 232–257
17. Momber AW, Kovacevic R (1997) Principles of abrasive water jet machining. Springer, Texas, pp 20–24
18. Hashish M (1989) Pressure effects in abrasive-waterjet (AWJ) machining. J Eng Mater Technol ASME 111:221–228
19. Manu R, Babu NR (2009) An erosion-based model for abrasive waterjet turning of ductile materials. Wear 266:1091–1097
20. Finnie I (1960) Erosion of surfaces by solid particles. Wear 3:87–103
21. Johnson GR, Holmquist TJ (1994) An improved computational constitutive model for brittle materials. In: Schmidt SC, Shaner JW, Samara GA, Ross M (eds) High-pressure science and technology, vol 309. AIP Publishing, New York, pp 981–984
22. Cronin DS, Bui K, Kaufmann C, McIntosh G, Berstad T, Cronin D (2003) Implementation and validation of the Johnson–Holmquist ceramic material model in LS-DYNA. In: Proceedings of 4th European LS-DYNA users conference, Ulm, Germany, pp 47–60
23. Hallquist JO (2006) LS-DYNA theory manual, Livermore software technology corporation, California, 19:142–143
24. Krashanitsa R, Shkarayev S (2005) Computational study of dynamic response and flow behavior of damaged ceramics. In: Proceedings of 46th AIAA/ASME/ASCE/AHS/ASC structures, structural dynamics, and materials conference, Austin, Texas, pp 1–8.
25. Anwar S, Axinte DA, Becker AA (2013) Finite element modelling of abrasive waterjet milled footprints. J Mater Process Technol 213: 180–193
26. Meo M, Vignjevic R (2003) Finite element analysis of residual stress induced by shot peening process. Adv Eng Softw 34:569–575
27. Meguid SA, Shagal G, Stranart JC (2002) 3D FE analysis of peening of strain-rate sensitive materials using multiple impingement model. Int J Impact Eng 27:119–134
28. Zurek AK, Meyers MA (1996) Microstructural aspects of dynamic failure. In: Lee D, Dennis EG, Mohsen S (eds) High-pressure shock compression of solids II. Springer, New York, pp 25–70
29. Ćurković L, Kumić I, Grilec K (2011) Solid particle erosion behaviour of high purity alumina ceramics. Ceram Int 37:29–35